Journal of Marine Science and Technology
https://doi.org/10.1007/s00773-025-01048-0

ORIGINAL ARTICLE

A practical and online trajectory planner for autonomous ships' berthing, incorporating speed control

Agnes N. Mwange[1,2] · Dimas M. Rachman[3] · Rin Suyama[1] · Atsuo Maki[1]

Received: 16 April 2024 / Accepted: 3 January 2025

Abstract
Autonomous ships are designed and equipped to perceive their internal and external environments and subsequently take appropriate actions based on predefined objective(s) without human intervention. Consequently, trajectory-planning algorithms for autonomous berthing must consider factors such as system dynamics, ship actuators, environmental disturbances, and operational safety. In this study, trajectory planning for an autonomous ship was modeled as an optimal control problem (OCP), which was transcribed into a nonlinear programming problem (NLP) using direct multiple shooting. To enhance berthing safety, wind disturbances, speed control guidelines, actuator limitations, and collision avoidance features were incorporated as constraints in the NLP, which was then solved using the sequential quadratic programming (SQP) algorithm in MATLAB. Finally, the performance of the proposed planner was evaluated through (i) comparison with an existing method, (ii) trajectory planning for different harbor entry and berth approach scenarios, and (iii) a feasibility study using predefined as well as stochastically generated initial conditions. The simulation results indicate improved berthing safety as well as practical and computational feasibility.

Keywords Autonomous berthing · Practical trajectory planning · Direct multiple shooting · Berth approach speed

1 Introduction

The berthing process can be categorized into two distinct phases: (i) the approach phase, spanning from harbor/port entry to the attainment of the docking pose, and (ii) the lateral alignment phase, involving crabbing maneuvers toward the final berthing position. During the approach phase, the ship undergoes controlled deceleration and navigates toward the docking pose - a position usually parallel and proximate to the berth. This maneuver is achieved either through direct control by the ship's captain or with the assistance of tugboats. Speed reduction during this phase is critical, as it significantly enhances operational safety [1] and mitigates the risk of collisions [2]. Per Rule 6 of the 1972 COLREGs, ships are required to operate at safe speeds that allow for the execution of emergency maneuvers without jeopardizing the safety of the ship, other ships, or structures [3]. In many ports, reduced speed zones (RSZs) are implemented, typically requiring ships to maintain a speed of approximately 10 knots in calm sea conditions. Noteworthy early research by Hara et al. [4] and Inoue et al. [1, 5] has contributed significantly to understanding deceleration patterns during the approach phase. Hara et al. proposed a deceleration model based predominantly on the operator's perception, while Inoue et al. introduced deceleration guidelines informed by the ship's braking capacity[5] and the operational experiences of ship masters [1]. On the other hand, the lateral alignment phase is characterized by minimal surge velocity and predominantly lateral motions as the ship transitions from the docking pose to the final berthing position. Due to the low surge velocity, the rudder's effectiveness is significantly diminished, necessitating alternative

✉ Agnes N. Mwange
mwange_agnes_ngina@naoe.eng.osaka-u.ac.jp

✉ Atsuo Maki
maki@naoe.eng.osaka-u.ac.jp

[1] Department of Naval Architecture and Ocean Engineering, Graduate School of Engineering, Osaka University, Suita, Osaka, Japan

[2] Department of Marine Engineering and Maritime Operations, Jomo Kenyatta University of Agriculture and Technology (JKUAT), P.O. Box 62000 - 00200, Nairobi, Kenya

[3] Intelligent Processing Technologies Laboratory, Furuno Electronic Co., Ltd, 8-1 Jingikan-cho, Nishinomiya 662-0843, Japan

Published online: 22 January 2025

methods for precise maneuvering. Consequently, this phase relies on alternative mechanisms, including mooring lines, tugboats, or side thrusters, to ensure precise alignment and positioning of the ship at the berth. Berthing operations can be performed through manual, semi-autonomous, or fully autonomous methods, each with its distinct advantages and limitations. Manual berthing, while providing flexibility and adaptability in unpredictable situations, is associated with human error, which accounts for approximately 50% of the marine accidents and incidents [6]. In contrast, autonomous berthing, which utilizes sophisticated algorithms to compute and execute optimal trajectories, presents a promising alternative to mitigate the challenges associated with manual berthing. The successful implementation of fully autonomous berthing, however, requires the development and integration of sophisticated guidance, navigation, and control (GNC) systems [7]. This study focuses on guidance systems, with a particular emphasis on trajectory planning for the approach phase of berthing, as a key component for the realization of autonomous berthing.

1.1 Related research

Trajectory planning for autonomous berthing can be considered a constrained nonlinear optimization problem that necessitates determining the optimal inputs that will steer the ship from an arbitrary position to the desired berthing position, taking into account the ship dynamics, desired objective(s), path constraint(s), and, where possible, environmental disturbances. Solving this optimization problem to generate dynamically and practically feasible states and control trajectories is a testament to successful trajectory planning. Despite its significance, only about 1% of trajectory planning algorithms focus on autonomous berthing [8], underscoring the need for further research to enhance its practical application.

Algorithms for path and trajectory planning fall into two categories: (i) local optimization, and (ii) global optimization [9]. These methods have been applied separately or combined for effective berthing solutions. The A* algorithm [10, 11], a global optimization method, has been adapted for improved collision avoidance [12], smoothness, and traceability [13]. While effective, the algorithm's performance depends on the quality of the heuristic function. Another approach involves customizing optimization algorithms for trajectory optimization. Maki et al. [14] proposed a berthing trajectory optimization algorithm based on the covariance matrix adaptation evolution strategy (CMA-ES)-based [15], with inequality constraints addressed [16], but without accounting for environmental disturbances. Later modifications by Miyauchi et al. [17] included wind disturbance considerations and the introduction of a ship domain for enhanced safety margin. CMA-ES was later adapted by Suyama et al. [18] to replicate captain maneuvers at a port. However, CMA-ES is computationally expensive, limiting its use to offline applications.

Local optimization methods have been key in automating the berthing process. Early work by Koyama et al. [19] and Yamato et al. [20] introduced knowledge-based and expert system planners for handling disturbances, respectively. Later, Shouji et al. [21] formulated the problem as a nonlinear two-point boundary value problem (TPBVP), solved using the sequential conjugate gradient restoration algorithm (SCGRA) [22], while Djouani et al. [23] used the discrete Augmented Lagrangian approach to minimize berthing time and energy while accounting for system dynamics and disturbances. Additionally, the Artificial Potential Field (APF) algorithm [24] has been adapted for collision avoidance [25] and smoother heading control [26], highlighting its potential for improved real-time performance and COLREGs compliance. Other approaches include nonlinear model predictive control (NMPC) as demonstrated by Mizuno et al. [27] and Zhang et al. [28], in which the latter prioritizes minimal berthing time but did not address collision avoidance or environmental factors. Martinsen et al. [29] used collocation-based planners with NMPC for improved real-time performance.

Combining global and local optimization algorithms has significant potential, where solutions from global optimization methods serve as warm-starts for local optimization, thereby improving accuracy and computational efficiency. The trajectory optimization problem is typically posed as an optimal control problem (OCP) and transcribed into nonlinear programming problem (NLP), then solved appropriately. Bitar et al. [30] refined A* solutions using direct collocation, while Rachman et al. [31] and Wang et al. [32] used CMA-ES and Hybrid A* solutions, respectively, as warm starts for the NLPs.

Current path and trajectory planning algorithms, while achieving notable performance, still present critical gaps in addressing navigation safety comprehensively [8]. A key limitation is the insufficient consideration of environmental disturbances [33], which compromises practical applicability in scenarios where disturbances exceed the ship's actuation capacity. Moreover, despite evidence that speed reduction significantly decreases accident frequency [34] as well as facilitates a smoother transition between the two phases of berthing [35], speed reduction criteria remain absent from existing trajectory optimization algorithms. Addressing these gaps is essential for improving the safety and reliability of autonomous berthing operations.

1.2 Objective and scope

The primary objective of this study is to enhance berthing safety by considering essential factors such as speed

reduction, external disturbances, and practical feasibility in trajectory optimization. The trajectory optimization problem was modeled as a minimum-time optimal control problem (OCP), transcribed into a nonlinear programming problem (NLP) using direct multiple shooting, and solved using the `fmincon` solver, `SQP` algorithm in MATLAB. The contributions of this study are as follows:

(i) An online optimal-control-based planner that uses a simple linear guess (linear interpolation between the initial and terminal optimization variables) to initialize the SQP algorithm,
(ii) Enhancement of practical feasibility by considering wind disturbances, spatial constraints, and imposing an artificial limit on the actuators,
(iii) Incorporation of speed reduction guidelines into the planner, and
(iv) Reasonable computational cost that makes the planner suitable for re-planning and potentially real-time applications.

To validate the algorithm, the optimal trajectories, states, and control obtained using the proposed planner were compared with those obtained using the CMA-ES algorithm for two different model ships: Ship A and Ship B. Ship A is a single screw model ship equipped with a bow thruster and vectwin rudder system, whereas Ship B is an underactuated model ship, as detailed in Table 1.

The remainder of the paper is organized as follows: Sect. 1.3 introduces the important notations used in the study; Sect. 2 introduces the model ship and its mathematical model. The section then describes the OCP to be solved, the transcription of the OCP into an NLP, and the detailed description of the NLP constraints. The transcription, actuator, speed reduction, and collision avoidance constraints are described here. This section also describes the simulation conditions used to validate and demonstrate the algorithm's performance; Sect. 3 presents the simulation results and the feasibility study; The outcomes of the study are discussed in Sect. 4 and concluded in Sect. 5.

Table 1 Principal particulars of model ships

	Ship A	Ship B
Length, L	3.0m	3.0m
Breadth, B	0.4m	0.4m
Draft, d	0.17m	0.17m
Propeller	1 fixed pitch propeller	1 fixed pitch propeller
Rudder	Vectwin rudder system	Single rudder
Side Thrusters	1 fixed pitch bow thruster	

1.3 Notations

In this study, $\mathbb{R}^n$ denotes the n-dimensional Euclidean space, where each coordinate is a real number. The terms marked with an asterisk (*) indicate the corresponding optimal values.

2 Methods

Ship A is the subject ship used in this study and its principal particulars are listed in Table 1.

2.1 Maneuvering model of the ship

In this study, the Maneuvering Model Group (MMG) harbor maneuvering model [36] was used to calculate the forces acting on the hull. The kinematic ship model used is a 3-DOF model that uses two coordinate systems: the earth-fixed system $O_0 - x_0, y_0, z_0$ and the ship-fixed system $O - x, y, z$ where O is the ship's center of gravity as shown in Fig. 1.

U_T is the speed of the true wind and γ_T is the direction of the true wind positive in the clockwise direction starting from the x-axis of the earth-fixed coordinate system. β is the ship's drift angle measured in the ship-fixed coordinate system. ψ, u_s, v_m, and r denote the ship's yaw angle, surge velocity, sway velocity, and yaw velocity, respectively. $U = \sqrt{u_s^2 + v_m^2}$, is the resultant ship speed.

Further, Eq. 1 describes how the kinematics at the midship can be transformed from the ship-fixed coordinate system to the earth-fixed coordinate system.

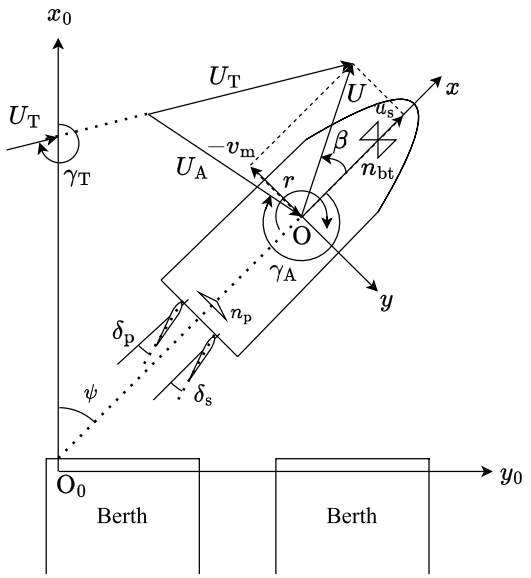

Fig. 1 Coordinate systems

$$\begin{bmatrix} \dot{x}_0 \\ \dot{y}_0 \\ \dot{\psi} \end{bmatrix} = \begin{bmatrix} \cos\psi & -\sin\psi & 0 \\ \sin\psi & \cos\psi & 0 \\ 0 & 0 & 1 \end{bmatrix} \begin{bmatrix} u_s \\ v_m \\ r \end{bmatrix} \tag{1}$$

The equation of motion, shown in Eq. 2, is based on the MMG model proposed by [37].

$$\begin{aligned} (m+m_x)\dot{u}_s - (m+m_y)v_m r - x_G m r^2 &= X \\ (m+m_y)\dot{v}_m + (m+m_x)u_s r + x_G m\dot{r} &= Y \\ \left(I_{zG} + J_z + x_G m^2\right)\dot{r} + \left(v_m + u_s r\right)x_G m &= N_m, \end{aligned} \tag{2}$$

where m represents the ship's mass, while m_x and m_y denote added masses in the x-axis and y-axis, respectively. The term I_{zG} denotes the moment of inertia acting at the ship's center of gravity, x_G, whereas J_z represents the added moment of inertia. The terms X and Y correspond to the total surge and sway forces, respectively, while N_m represents the yaw moment about the midship. The right-hand side of Eq. 2 can be expanded as follows:

$$\begin{aligned} X &= X_H + X_P + X_{BT} + X_R + X_A \\ Y &= Y_H + Y_P + Y_{BT} + Y_R + Y_A \\ N_m &= N_H + N_P + N_{BT} + N_R + N_A \end{aligned} \tag{3}$$

The subscripts H, P, BT, R, and A denote hull, propeller, bow thruster, rudder, and air, respectively. Equation 3 summarizes the summation of the surge and sway forces and moments resulting from the hydrodynamic forces acting on the hull, steering forces and moments induced by the rudder, thrust forces and moments generated by the propeller and bow thruster, and wind forces and moments. The hydrodynamic forces and moments induced by the propeller thrust were expressed based on the Yasukawa et al. [37] model. Unlike conventional ships where the propeller can operate in both forward and reverse directions, propellers for ships equipped with a vectwin rudder system are operated in the forward direction only. The vectwin rudder system consists of a pair of rudders with specially designed profiles mounted symmetrically on the hull behind the propeller. The angle range for each rudder is 140^0, that is, 105^0 towards the outboard and 35^0 towards the inboard. This enables the ship to perform common maneuvers such as turning, emergency stop, and crash-astern by maintaining a constant forward propeller revolution and a desirable combination of rudder angles. The rudders can be operated as a pair or individually as in a conventional twin rudder ship. The forces and moments induced by the rudder were formulated as described by Kang et al. [38]. The forces and moments due to the wind (air) were calculated using the method presented by Fujiwara et al. [39].

From Eq. 2, the expressions for mass and added masses can be simplified as, $M_x = m + m_x$ and $M_y = m + m_y$. In addition, the expression $(I_{zG} + J_z + x_G^2 m)$ was simplified to I_{zm}. Subsequently, Eq. 2 can be rewritten as:

$$\begin{aligned} \dot{u}_s &= \frac{(X + M_y v_m r + x_G m r^2)}{M_x} \\ \dot{v}_m &= \frac{(Y - M_x u_s r)I_{zm} - (N_m - x_G m u_s r)(x_G m)}{M_x I_{zm} - (x_G m)^2} \\ \dot{r} &= \frac{(Y - M_x u_s r)(x_G m) - (N_m - x_G m u_s r)M_y}{(x_G m)^2 - M_y I_{zm}} \end{aligned} \tag{4}$$

2.2 Trajectory optimization and formulation

2.2.1 Optimal control problem (OCP)

System dynamics as shown in Eq. 5 were obtained by combining Eqs. 1 and 4.

$$\dot{x}(t) = f(x(t), u(t), U_T, \gamma_T), \tag{5}$$

where U_T and γ_T are the true wind speed and direction, respectively. For the trajectory planner, the wind parameters were estimated at the beginning and were assumed to be steady throughout the trajectory. Let $\bar{t}$ be the actual time outside the planner. The wind parameters were estimated at time $\bar{t}_j$, corresponding to t_0 of the planner.

The states vector is defined as:

$$x(t) \equiv [x_0, y_0, \psi, u_s, v_m, r]^\intercal \in \mathbb{R}^6, \tag{6}$$

where x_0 and y_0 denote the earth-fixed position in the x and y directions, respectively.

The control vector is defined as:

$$u(t) \equiv [\delta_p, \delta_s, n_p, n_{bt}]^\intercal \in \mathbb{R}^4, \tag{7}$$

where δ_p, δ_s, n_p and n_{bt} denote the port rudder, starboard rudder, propeller, and bow-thruster, respectively. Let t_0 and t_f denote the initial and final times, respectively. The corresponding initial and final states are expressed as $x(t_0) = x_0$ and $x\left(t_f\right) = x_f$, respectively.

The OCP to be solved is the minimum-time berthing problem, which is defined by the objective function presented in Eq. 8.

$$\begin{aligned} &\text{minimize } J = \sum_{i=1}^{6} \|x_i\left(t_f\right) - x_{f,i}\|^2 \times \int_0^{t_f} \sum_{i=1}^{6} \|x_i(t) - x_{f,i}\|^2 \mathrm{d}t \\ &\text{subject to } t \in [0, t_f] \text{ and } t_f \in (0, \infty) \\ &\dot{x}(t) = f(x(t), u(t), U_T, \gamma_T) \\ &x^*(t_0) = x_0 \\ &x^*\left(t_f\right) = x_f \\ &u_{\min} \le u(t) \le u_{\max}. \end{aligned} \tag{8}$$

The objective function was originally proposed by Maki et al. [40] and later modified for optimization using SQP by Rachman et al.[31].

2.2.2 Discretization and transcription

This study utilized direct multiple shooting, one of three direct numerical methods for solving OCPs [41]. This approach was chosen based on the evidence that it offers superior accuracy and computational efficiency[42–44]. To discretize the continuous-time optimal control problem and transcribe it into a nonlinear programming problem (NLP), the trajectory with time interval $[0, t_f]$ is divided into N_s segments (Fig. 2). Let i denote the i_{th} segment such that, $i = 1, 2, \ldots, N_s$. The endpoints of the segments act as discretization points and are hereafter known as *knots*. Let N_k denote the number of knots such that $k = 1, 2, \ldots, N_k$, where k denotes the k_{th} knot point. In addition, $N_k = N_s + 1$.

The command control input per segment is approximated as piecewise constant, measured at knot points, $u_k \equiv u(t_k)$. The actual control input in the planner incorporates actuator rate changes and is saturated at the command input value, as shown in Eq. 2. The rate of change is based on actual actuator data. Limiting the control input deliberately enhances berthing safety by creating a buffer zone to counter unknown disturbances [45]. Henceforth, in this study, only 43% of the rudders', 50% of the propeller, and 75% of the bow thruster actuation were used.

For any segment i starting from k to $k+1$ knot points, the states $x_k \equiv x(t_k)$ and control u_k obtained from each iteration are used to integrate the system equations of motion, (true dynamics), $f_T(t_k)$ over that segment using the 4th order Runge–Kutta scheme.

$$x_T(t_{k+1}) = \int_{t_k}^{t_{k+1}} f_T\big(x(t_k), u(t_k), U_T(\bar{t}_j), \gamma_T(\bar{t}_j)\big)\mathrm{d}t \tag{9}$$

The 'true states', $x_T(t_{k+1})$ obtained from equation Eq. 9 at the end of the segment are compared with the computed states obtained from the SQP solver, x_{k+1}. Ideally, these states should match. This condition, expressed in Eq. 10, refers to the quadrature constraints and is included as part of the equality constraints in the NLP.

$$x_{k+1} = x_T(t_{k+1}) \tag{10}$$

To ensure continuity between segments and minimize the defects, the states at the end of one segment, x_{k^-}, must match the states at the beginning of the subsequent segment, x_{k^+}. This condition is expressed in Eq. 11 and serves as an equality constraint in the NLP.

$$x_{k^-} = x_{k^+} \tag{11}$$

2.2.3 Speed reduction criterion

In this study, the speed reduction guidelines proposed by Inoue et al. [1] were incorporated into the trajectory planner. The developed guidelines consider both operational safety and captains' perceptions of safety, where each region represents a certain safety status. As shown in Fig. 3, if a ship operates within the '**Red**' region, it cannot achieve zero speed before reaching the target berthing point even if Full Astern braking force is used. Although it is possible to stop the ship using Full Astern, Astern, or Slow Astern braking force, operating within the '**Amber**' region poses a high risk of losing control of the ship. Within the '**Available**' regions, the captain can use Dead Slow Astern or Slow Astern braking force and easily change

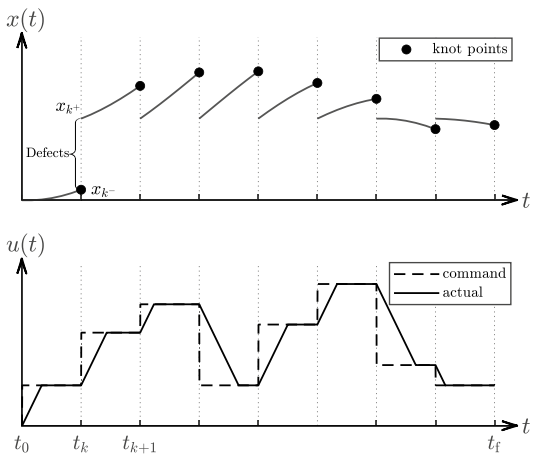

Fig. 2 Illustration of direct multiple shooting

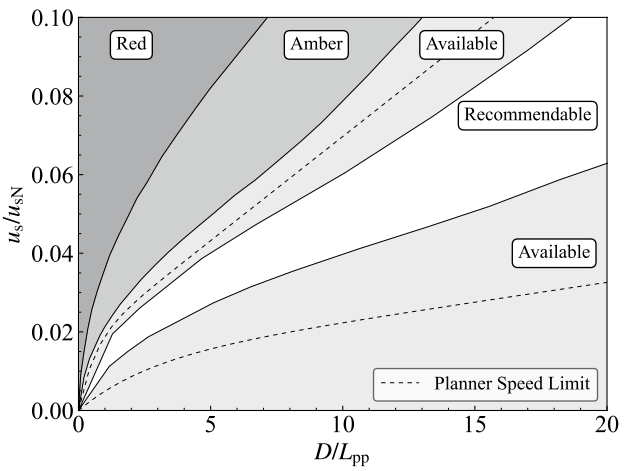

Fig. 3 Speed reduction criterion based on guidelines proposed by Inoue et. al [1]

the ship's course without the risk of losing control. According to the questionnaire data, most captains operate within the '**Recommendable**' region with Dead Slow Astern braking force. For more information, refer to Figs. 3 and 4.

In previous trajectory planning algorithms, speed reduction guidelines were not considered. As illustrated in Fig. 5, some trajectories resulting from these earlier algorithms [31, 40] depict the ship nearing the berth within the '**Amber**' region, and dangerously close to the '**Red**' region. This increases the risk of losing navigational control. In addition, the presence of environmental disturbances would significantly increase the risk of collision or contact with port structures. Subsequently, this study addressed this challenge by introducing speed limits, which would maintain the ship close to the '**Recommendable**' region.

This study used guidelines proposed by Inoue et al. [1] to derive the speed reduction criterion, and the desired minimum and maximum speed limits were defined as shown in Fig. 3. The terms u_s, u_{sN}, and D denote the ship's forward speed in m/s, nominal ship speed in m/s, and the ship's distance from the berth in meters, respectively. Equation 12 defines the correlation between the desired speed limits and the ship's distance from the berth.

$$u_{d(\min,\max)} = c_1 d + c_2(1 - e^{-c_3 d}), \tag{12}$$

where u_d denotes the non-dimensional ship's forward speed when it is at a nondimensional longitudinal distance d from the final berthing point, such that, $u_d = u_s/u_{sN}$ at a distance $d = D/L_{pp}$ from the berth. The values of coefficients c_1, c_2 and c_3 are listed in Table 2.

Equation 13 forms part of the inequality constraints in the NLP, such that, for all knot points,

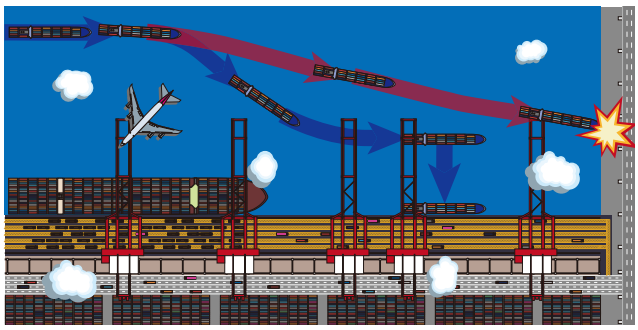

Fig. 4 A schematic aerial view of a port layout that summarizes the speed reduction guidelines proposed by Inoue et al. [1]. It depicts two berthing scenarios: (1) The scenario where the ship approaches the berth at a reduced/controlled speed (blue path) and reaches the berth safely. Along this path, the braking force may be as low as Dead Slow Astern or as high as Full Astern. (2) In the second scenario, the ship approaches the berth at a high speed (red path), and even with Full Astern as the braking force, the ship is unable to stop at the desired berth and subsequently collides with the pier, jetty, or wall

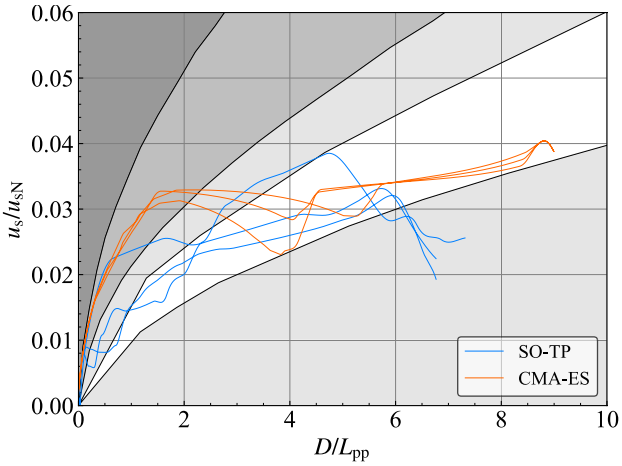

Fig. 5 Berth approach speed trends of trajectories generated using the CMA-ES algorithm [40] and the semi-online trajectory planner (SO-TP) [31]

$$u_{d(\min)}(t_k) \leq u_s(t_k) \leq u_{d(\max)}(t_k) \tag{13}$$

2.2.4 Collision avoidance constraints

Solving the point-in-polygon (PIP) problem is a fundamental method for assessing the spatial relationship between two objects. In this study, the winding number method [46] was employed to define collision avoidance constraints, treating the port layout as a closed 2D planar polygon and the vertices of the ship domain as points whose inclusion in the polygon is to be determined. Rachman et al. [31] demonstrated the effectiveness of this approach in defining spatial constraints within trajectory optimization. The ship domain represents the effective 2D region surrounding the ship that must remain clear of other ships or port structures. The shape and size of the ship domain are influenced by factors such as ship dimensions, maneuverability, environmental conditions, and speed. In this study, an elliptical ship domain was employed, with its dimensions dependent on the ship's length, breadth, and speed as proposed by Miyauchi et al. [17].

The shape and position of the port boundary vertices are derived from the topography of Inukai Pond at Osaka University. Only the relevant section of the pond, both depthwise and within $20L_{pp}$ with additional space, was considered,

Table 2 Coefficients of the speed limits equation

Coefficient	Lower speed limit	Upper speed limit
c_1	1.0×10^{-3}	5.3×10^{-3}
c_2	1.26×10^{-2}	1.67×10^{-2}
c_3	3.72×10^{-1}	1.67

reflecting the typical maneuvering area during berthing or unberthing operations, as shown in Fig. 6. The coordinates of these vertices were recorded in the earth-fixed coordinate system, with the area enclosed by the polygon considered free of obstacles.

Let N and $\mathbf{P}_i$ denote the number of port boundary vertices and the i_{th} vertex of the port boundary, respectively, such that $i = 1, \ldots, N$. N_{sd} denotes the number of ship-domain vertices, and $\mathbf{Q}_j$ is the j^{th} vertex of the ship domain such that $j = 1, \ldots, N_{\text{sd}}$. Let θ_i be the angle subtended from the j_{th} vertex of the ship domain by two consecutive vertices of the port boundary; $\mathbf{P}_i$ and $\mathbf{P}_{i+1}$. Refer to Fig. 7 for more information.

At each knot point, the winding number $\mathbf{wn}(\mathrm{Q}_j, \mathbf{P})$, which represents the sum of the angles θ_i, subtended from each ship domain vertex and all port boundary vertices was computed as outlined in Eq. 14 and incorporated into the NLP equality constraints.

$$\mathbf{wn}(\mathbf{Q}_j, \mathbf{P}) = \sum_{i=1}^{N} \theta_{j,i}\Big|_k \tag{14}$$

2.2.5 Finite dimension NLP

Since the ship is operated with constant propeller revolutions, n_{p} was excluded from the optimization variables. The vector of unknown variables, $\mathbf{X}$, to be optimized is expressed as:

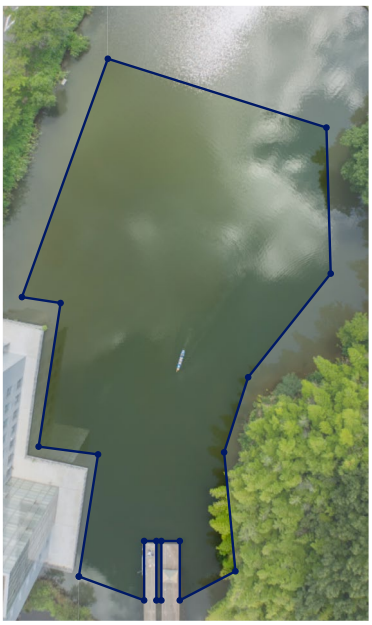

Fig. 6 Port geometry relative to Inukai Pond at Osaka University

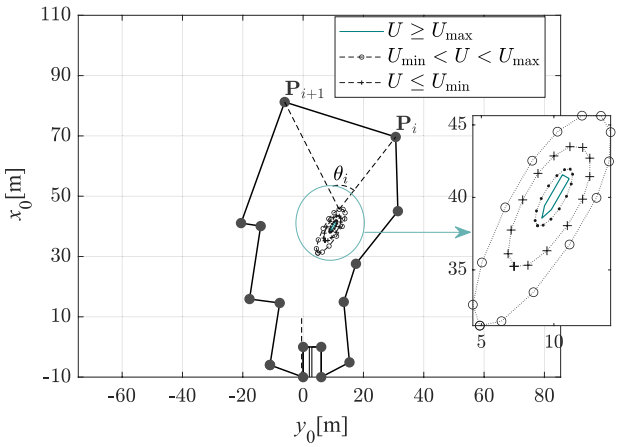

Fig. 7 Port boundary and ship domain vertices

$$\mathbf{X} \equiv (t_{\text{f}}, x_1, \ldots, x_{N_k}, u_1, \ldots, u_{N_k-1})^{\intercal} \in \mathbb{R}^{N_k+(N_k-1)+1} \tag{15}$$

The OCP to be solved was transcribed into a finite dimension NLP, incorporating additional constraints, and defined as:

$$\text{minimize} J = \sum_{i=1}^{6} \|x_i(t_{\text{f}}) - x_{\text{f},i}\|^2 \times \int_0^{t_{\text{f}}} \sum_{i=1}^{6} \|x_i(t_k) - x_{\text{f},i}\|^2 \mathrm{d}t$$

subject to

$$\begin{aligned}
&t_k \in [0, t_{\text{f}}] \ \text{ and } \ t_{\text{f}} \in (0, \infty)\\
&U_{\text{T}}(t_k) = U_{\text{T}}(\bar{t}_j) \text{ and } \gamma_{\text{T}}(t_k) = \gamma_{\text{T}}(\bar{t}_j) x^*(t_0) = x_0\\
&x^*(t_{\text{f}}) = x_{\text{f}}\\
&x_k^- = x_k^+ \ \text{ for } \ k = 2, \ldots, N_k\\
&x_{k+1} = x_{\text{T}}(t_{k+1}) \ \text{ for } \ k = 2, \ldots, N_k\\
&u_{\text{d(min)}}(t_k) \ \leq \ u_{\text{s}}(t_k) \ \leq \ u_{\text{d(max)}}(t_k) \ \text{ for } \ k = 1, \ldots, N_k\\
&\sum_{i=1}^{N} \theta_{j,i}\Big|_k = 2\pi \ \text{ for } \ j = 1, \ldots, N_{\text{sd}} \ \text{ and } \ k = 1, \ldots, N_k\\
&u_{\min} \leq u(t_k) \leq u_{\max}\\
&n_{\text{p}}(t_k) = 10\text{rps}.
\end{aligned} \tag{16}$$

The flow chart shown in Fig. 8 summarizes the optimization process described in Sect. 2.2.

2.3 Simulation conditions

The approaches to harbors and berths by a ship are governed by a complex interplay of factors, including port regulations, prevailing wind conditions, tidal currents, ship dimensions, and maneuverability limitations. In this study, a virtual harbor entrance was introduced, as illustrated in Fig. 9, to simulate realistic scenarios of harbor entry and berth approach without recomputation attempts. Six cases were analyzed, encompassing head-on and oblique

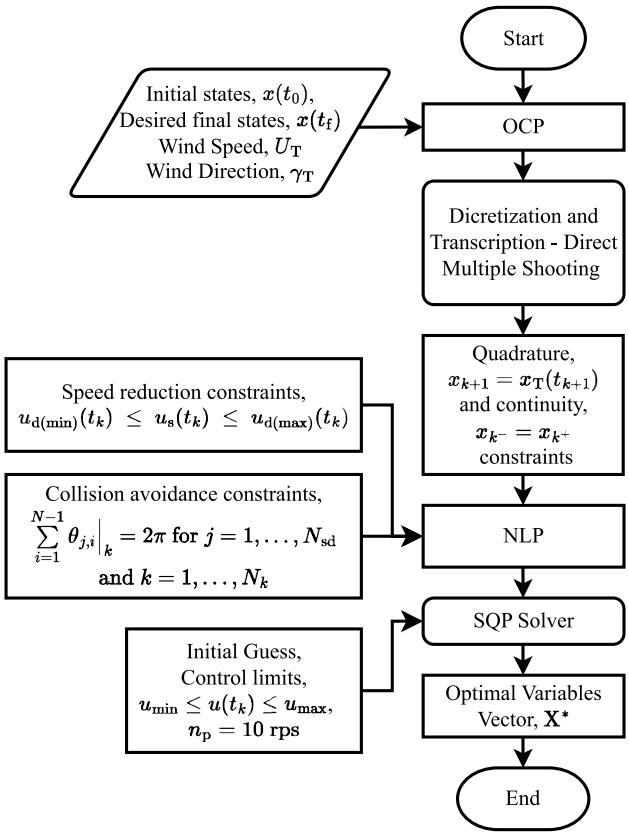

Fig. 8 Flow chart of the optimization process

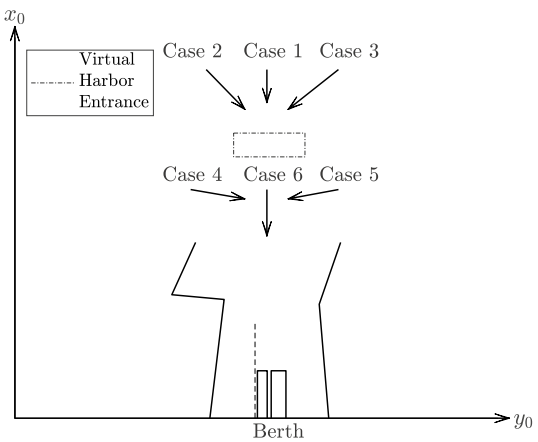

Fig. 9 Simulation cases

approaches to the harbor entrance, as well as parallel and angular approaches to the berth, thereby capturing a range of operational conditions.

The initial states and wind conditions for each case are detailed in Table 3, while Table 4 provides a summary of other simulation parameters, and computer and software specifications.

3 Computation results

3.1 Comparison with an existing method

The accuracy and reliability of the proposed planner are demonstrated by comparing the optimal trajectories obtained with those obtained using the CMA-ES algorithm [40], for two different model ships. The simulation was performed without recomputation attempts. The initial and final states $x(t_0)$ and $x(t_f)$ for the SQP were set to be similar to those of the CMA-ES algorithm. As shown in Fig. 10a and b, when the CMA-ES solution was used to initialize the SQP, the optimal trajectories obtained were nearly identical to those obtained using CMA-ES.

3.2 Simulation cases

3.2.1 Case 1: Head-On approach to the harbor entrance

In this scenario, the ship approaches a harbor or port directly from the open sea, aligning its bow with the entrance of the harbor such that the longitudinal axis of the ship is perpendicular to the entrance. This approach is suitable for ships with great course-keeping abilities under calm environmental conditions. In the simulation, the ship is initially positioned $20L_{pp}$ away from the berth, with the relative wind blowing from its starboard side. The optimal trajectories obtained with and without speed reduction constraints are shown in Fig. 11. Notable variations in the trajectories are evident past the harbor entrance. Ultimately, within a $2L_{pp}$ range from the berth, the absence of speed reduction constraints results in the ship approaching the berth within the '**Amber**' region.

3.2.2 Case 2: Oblique approach to the harbor entrance

In this scenario, the ship is not directly aligned with the entrance but approaches at an angle, that is, the ship's longitudinal axis forms an angle with the imaginary line perpendicular to the harbor entrance. This approach helps counteract the impact of wind and strong currents and better manage the ship's stability in challenging weather conditions [47]. Similar to Case 1, the ship is initially positioned approximately $20L_{pp}$ away from the berth, with the relative wind blowing from its starboard side. However, in Case 2, the initial lateral position of the ship is offset by 6.5m to the starboard side of the initial lateral position of the ship in Case 1. The optimal trajectories obtained with and without speed reduction constraints are shown in Fig. 12. The trajectories and deceleration patterns of the solutions exhibit a marked degree of similarity. However, similar to what was

Table 3 Initial conditions for the simulation cases

Case	Initial states						Wind	
	$x(t_0)$						$(t = \bar{t}_j)$	
	x_0	u_s	y_0	v_m	ψ	r	γ_T	U_T
	[m]	[m/s]	[m]	[m/s]	[rad]	[rad/s]	[deg]	[m/s]
1	60	0.70	0	0	3.14	0	45	0.75
2	60	0.70	− 6.5	0	2.67	0	315	0.75
3	60	0.70	6.5	0	3.61	0	250	0.75
4	30	0.35	− 6.5	0	2.20	0	135	0.25
5	30	0.35	6.5	0	4.08	0	225	0.25
6	30	0.35	0	0	3.14	0	225	0.25

Table 4 Simulation conditions

Distance from the berth	$0 \leq D \leq 20L_{pp}$
Forward velocity	$u_s \leq 0.75$ m/s. This corresponds to about 10 knots of the full-scale ship
Computer used	16GB RAM and Intel(R) Core(TM) i7-9700 CPU @ 3.00GHz 8-core Processor
MATLAB	R2019b, `fmincon` solver, `SQP` algorithm

observed in Case 1, within the $2L_{pp}$ range from the berth, the lack of speed constraints leads to the ship approaching the berth within the '**Amber**' region.

3.2.3 Case 3: Oblique Approach to the Harbor Entrance

This scenario is similar to Case 2 but the ship approaches from the opposite side of the harbor entrance, with the initial lateral position of the ship offset by 6.5 m to the port side of the initial lateral position in Case 1. The initial position of the ship is approximately $20L_{pp}$ away from the berth, with the relative wind blowing from its starboard side. Further, this approach helps reduce the risk of accidents or difficulties when entering a harbor [47]. The optimal trajectories obtained with and without speed reduction are shown in Fig. 13. The differences in trajectories and deceleration patterns between solutions with and without speed constraints become apparent past the harbor entrance, closely resembling the patterns observed in Case 1. These similarities extend to the relative wind direction as well. As observed in previous cases, in the absence of speed constraints, the ship approaches the berth within the '**Amber**' region when within the $2L_{pp}$ range.

3.2.4 Case 4: Angular approach to the berth

In this scenario, the orientation of the ship with respect to the berth is such that its longitudinal axis is at an angle to the berth. This approach is common in the presence of currents and winds or for large ships operating in confined harbor areas. In Case 4, the ship is initially positioned approximately $10L_{pp}$ away from the berth with a lateral position of the ship similar to Case 2 and relative wind blowing from its starboard side. The initial heading of the ship, in this case, is sharper compared to Case 2, and the initial speed is approximately half of the initial speed in Case 2. The optimal trajectories obtained with and without speed reduction are shown in Fig. 14. The trajectories and deceleration patterns show significant similarity, closely resembling the patterns seen in Case 2, although in this case, the relative wind blows from a different direction. Despite the similar deceleration patterns, in the absence of speed reduction constraints, the ship enters the '**Amber**' region within $2L_{pp}$ from the berth.

3.2.5 Case 5: Angular approach to the berth

This scenario is similar to Case 4, but the ship approaches from the opposite side of the berth. In Case 5, the ship is initially positioned approximately $10L_{pp}$ away from the berth with a lateral position of the ship similar to Case 3 and relative wind blowing from its port side. The initial heading of the ship, in this case, is sharper compared to Case 3, and the initial speed is approximately half of the initial speed in Case 3. The optimal trajectories obtained with and without speed reduction are shown in Fig. 15. In both cases, the ship initially decelerates; however, in the absence of speed reduction constraints, the ship decelerates to a significantly low speed. While this speed places the ship within the '**Available**' region, such a low speed may impair the ship's ability to counteract external disturbances effectively. The ship subsequently accelerates to reach the berth and enters the '**Amber**' region when it is within $2L_{pp}$ of the berth. This highlights the potential risk

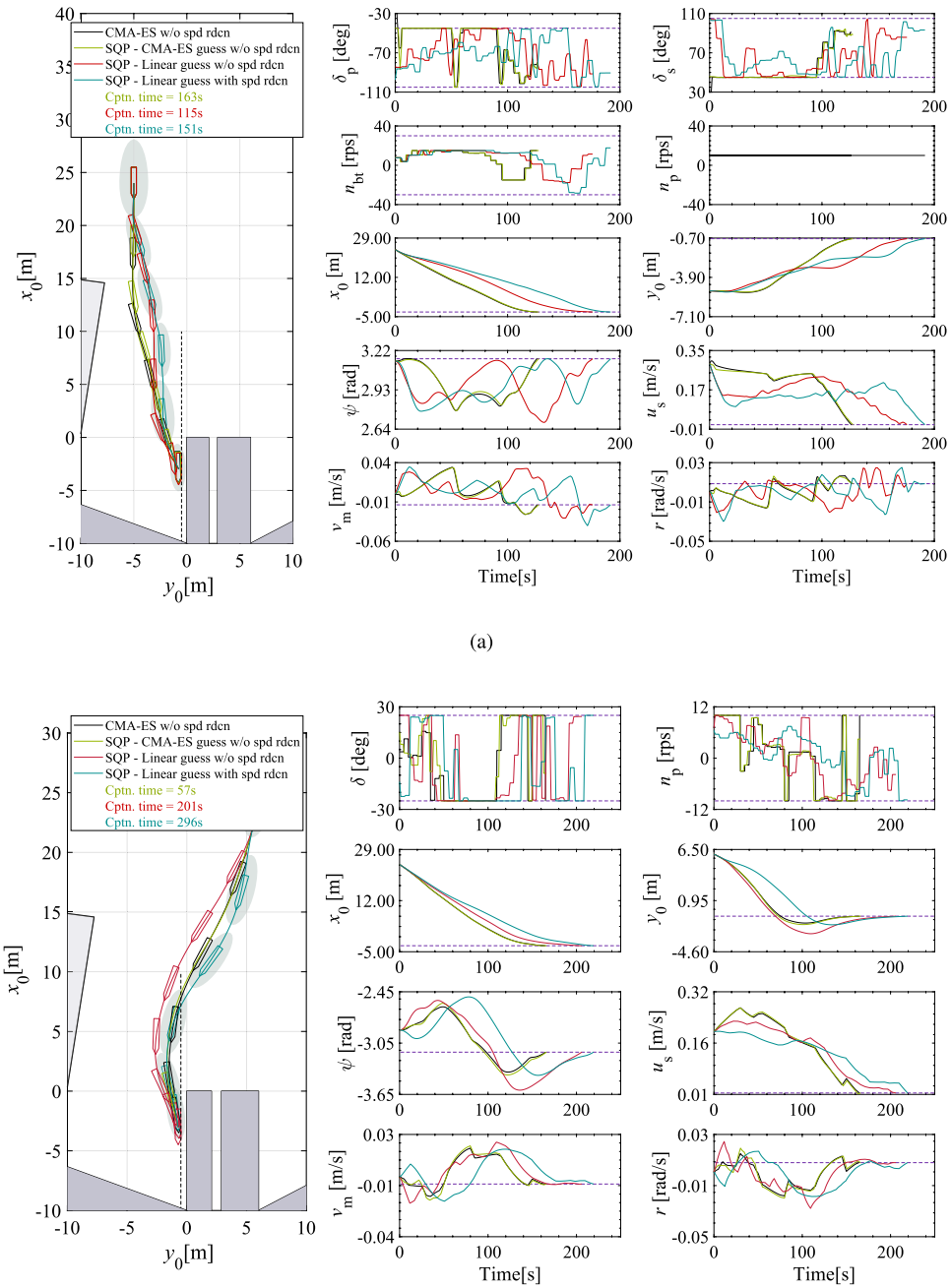

Fig. 10 A comparison of the optimal trajectories, controls, and states for **a** ship A and **b** ship B. The comparison is between four solutions: (i) CMA-ES solution without speed reduction (black), (ii) SQP solution initialized using the CMA-ES solution, without speed reduction (apple green), (iii) linearly initialized SQP solution, without speed reduction (red), and (iv) linearly initialized SQP solution, incorporating speed reduction (blue). It should be noted that this comparison did not take into account wind disturbances

posed by uncontrolled deceleration within the approach phase of berthing.

3.2.6 Case 6: Parallel approach to the berth

A parallel approach to the berth refers to the scenario in which the ship approaches the berth such that its longitudinal axis is aligned with the axis of the berth. This approach is suitable for ships with great course-keeping abilities and less congested harbor areas. Similar to Cases 4 and 5, in Case 6, the ship is initially positioned $10L_{pp}$ away from the berth, with the relative wind blowing from its foreside. The initial heading is similar to that in Case 1, and the initial speed of the ship is half of the initial speed in Case 1. The optimal trajectories obtained with and without speed reduction are shown in Fig. 16. Consistent with all previous cases, without speed constraints, the ship enters the '**Amber**' region when within a $2L_{pp}$ range from the berth. Although the initial orientations of the ship in Case 1 and

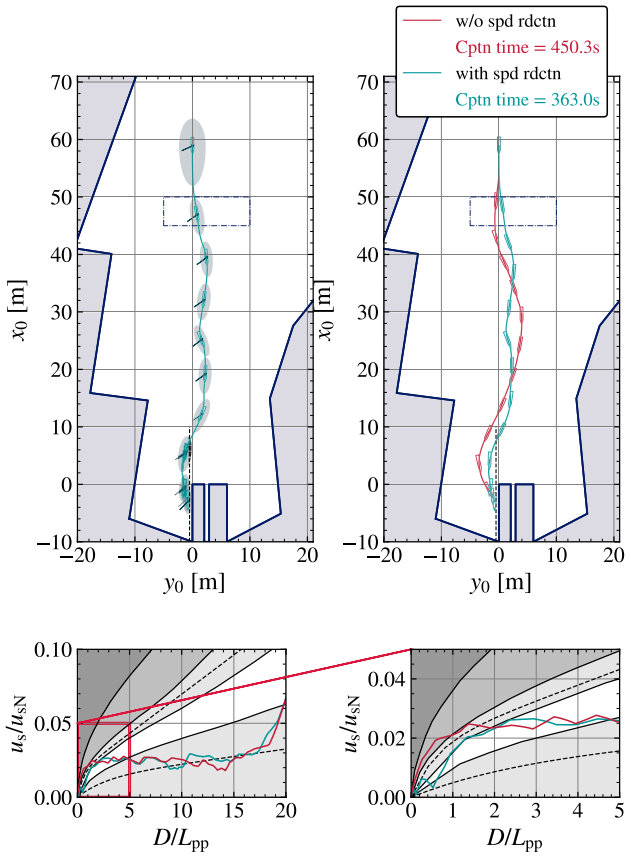

Fig. 11 Case 1: Optimal trajectory for a head-on approach to the harbor entrance in the presence of wind disturbances, that is, $U_T = 0.75$ [m/s], $\gamma_T = 45°$

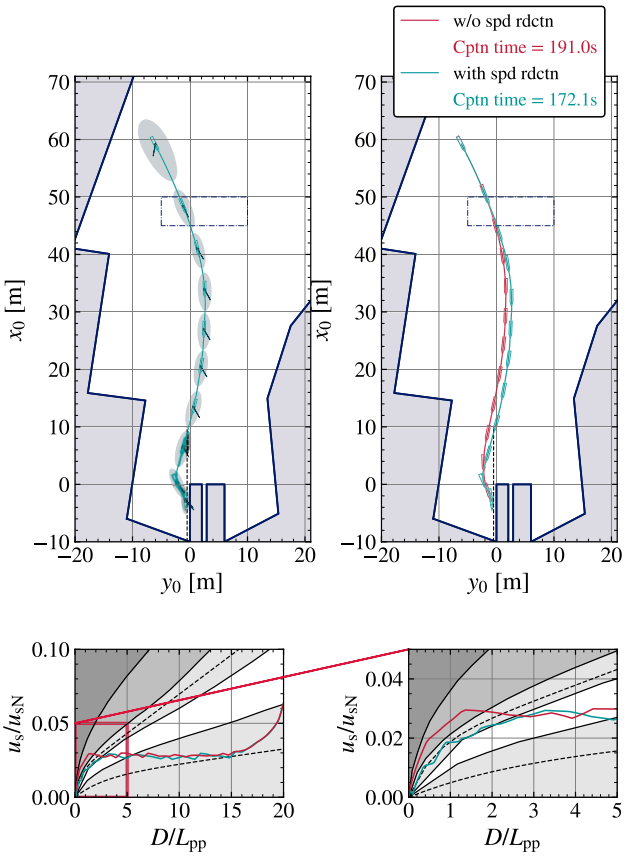

Fig. 12 Case 2: Optimal trajectory for an oblique approach to the harbor entrance in the presence of wind disturbances, that is, $U_T = 0.75$ [m/s], $\gamma_T = 315°$

Case 6 are identical, differences in the distance from the berth, speed, and wind conditions, influence the objective function and constraints to be satisfied, leading to solutions with different approach patterns.

3.3 Feasibility study

In the context of SQP, "feasible solution" refers to a solution that satisfies all constraints of the optimization problem. On the other hand, "infeasible solution" refers to the situation in which the SQP algorithm fails to find a solution that satisfies all constraints. In some instances, the SQP solver may terminate prematurely due to reaching a predefined maximum number of iterations. In this study, cases in which the solver stopped prematurely were categorized as infeasible.

The feasibility study was conducted using two distinct approaches:

(i) Grid-based simulations
(ii) Stochastic initial conditions

3.3.1 Grid-based simulations

The port geometry was discretized into a uniform grid, with the center of each grid cell serving as a representative position. For each position, simulations were conducted across four initial speeds $(0.150, 0.343, 0.535,$ and $0.723\text{m/s})$ for each of the three initial headings shown in Fig. 17. Subsequently, there were 12 simulation cases per grid square and the simulations were done once without recomputation.

A total of approximately 625 cases were simulated. As shown in Fig. 18, the distribution of feasible cases across the port geometry is illustrated. The distribution varies notably between the two simulations, with the simulation without speed reduction constraints yielding a higher number of feasible cases compared to the simulation incorporating speed reduction constraints.

It is important to note that, regardless of the presence of speed reduction constraints, most cases near the port wall were inherently infeasible due to violations of collision constraints, as the ship or its trajectory would inevitably intersect with the port boundaries. In scenarios with high initial speeds (0.723 m/s), the ship's domain expanded

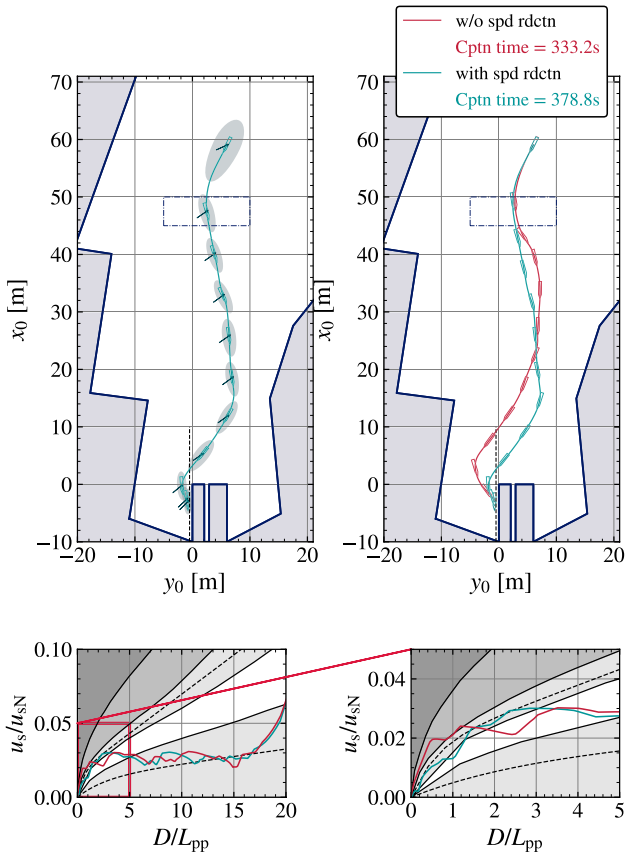

Fig. 13 Case 3: Optimal trajectory for an oblique approach to the harbor entrance in the presence of wind disturbances, that is, $U_T = 0.75$ [m/s], $\gamma_T = 45°$

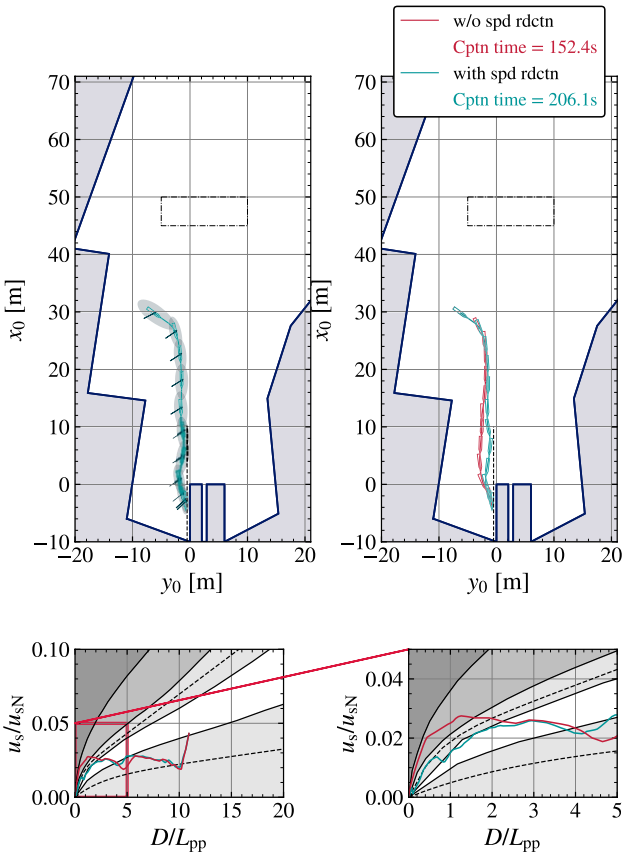

Fig. 14 Case 4: Optimal trajectory for an angular approach to the berth in the presence of wind disturbances, that is, $U_T = 0.25$ [m/s], $\gamma_T = 135°$

significantly, surpassing the limits of the port geometry and violating the collision constraints. Similarly, in other cases, the initial positions were so close to the port wall that, even at the lowest speed, the ship's domain would still extend beyond the port boundaries, thereby violating the collision constraints. These factors collectively contributed to the infeasibility of these cases.

In the context of feasibility distribution based on speed constraints, some cases were deemed infeasible from the outset in simulations with speed reduction constraints due to violation of speed constraints. This was not the case in simulations where speed constraints were absent, as such constraints did not apply. Furthermore, in scenarios where the initial speed was high but still within the planner's constraints, in simulations with speed reduction constraints, the control inputs must not only ensure the correct heading but also facilitate deceleration to satisfy the speed constraints. This differs from cases without speed reduction constraints, where the primary requirement for control inputs is to maintain the correct heading and achieve the appropriate deceleration to reach the set speed at the final position, without the additional constraint of adhering to a speed limit during the maneuver. These additional requirements in the simulations with speed reduction constraints are considered to have contributed to a higher number of infeasible cases compared to those without speed constraints.

Additionally, Fig. 19 illustrates the number of feasible cases that violate critical speed limits. In this figure, the lower speed limit corresponds to the proposed planner's lower speed limits, below which it is considered challenging for the ship to counteract wind and other environmental disturbances. The amber and red speed limits are based on the speed reduction guidelines by Inoue et al.[1]. In the absence of speed reduction constraints, approximately 26 trajectories of the feasible solutions fell within the amber region, and 14 trajectories were in the red region. This underscores the importance of incorporating speed reduction constraints to ensure safer trajectories. With the implementation of speed reduction constraints, only 2 trajectories of the feasible cases were found within the amber and red regions. This can be attributed to the distribution of knot points, where, although the speed at all knot points remained within the prescribed speed constraints, certain instances along the trajectory segments violated the constraints. Such

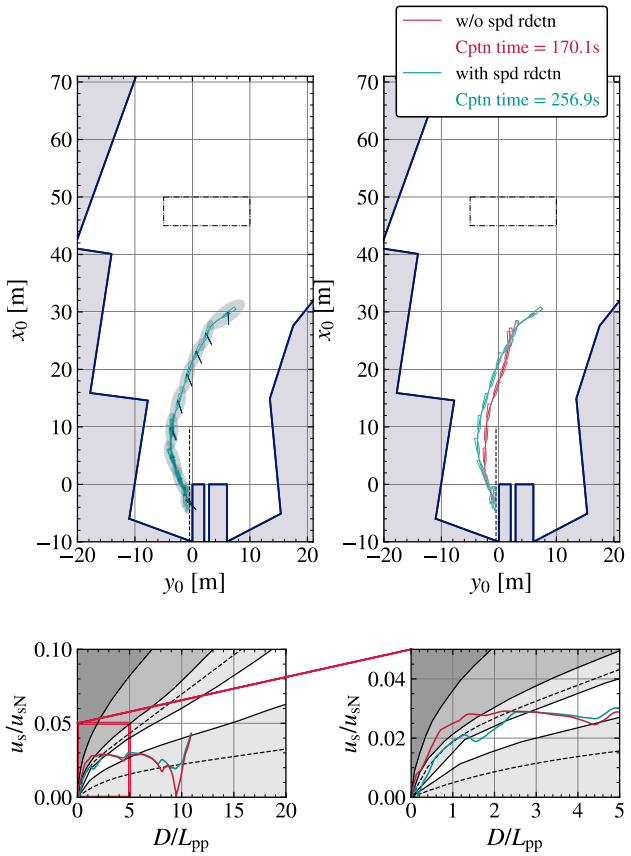

Fig. 15 Case 5: Optimal trajectory for an angular approach to the berth in the presence of wind disturbances, that is, $U_T = 0.25$ [m/s], $\gamma_T = 225°$

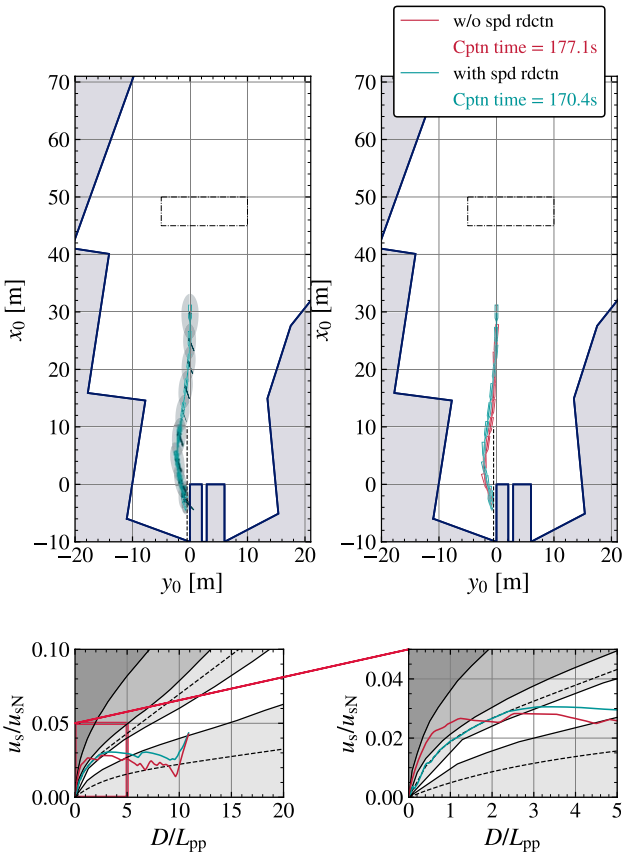

Fig. 16 Case 6: Optimal trajectory for a parallel approach to the berth in the presence of wind disturbances, that is, $U_T = 0.25$ [m/s], $\gamma_T = 225°$

violations could potentially be mitigated by increasing the number of segments, allowing for more precise control over the speed at intermediate points. However, this approach would likely result in a significant increase in computational load, presenting a trade-off between safety and computational efficiency.

3.3.2 Stochastic initial conditions

This approach involved the assessment of 200 cases with stochastically generated initial conditions within predefined bounds to ensure practicality and realistic operational scenarios. Further, a maximum of three recomputation attempts were made with different control input initializations for the cases initially deemed infeasible.

Initially, solutions to 100 cases, (50%) out of 200 cases considered were found feasible, as shown in Fig. 20. The number of feasible cases increased to 125 (62.5%), 142 (71%), and 151 (75%) after the first, second, and third recomputation attempts, respectively, as shown in the figure, Fig. 20.

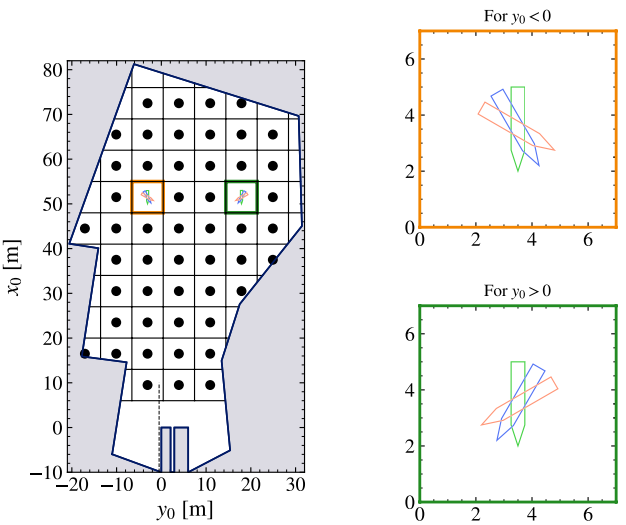

Fig. 17 Distribution of grid squares across the port geometry. The grid squares highlighted in green and orange are magnified and displayed in the side plots, with their axes color-coded to match the corresponding grid highlights

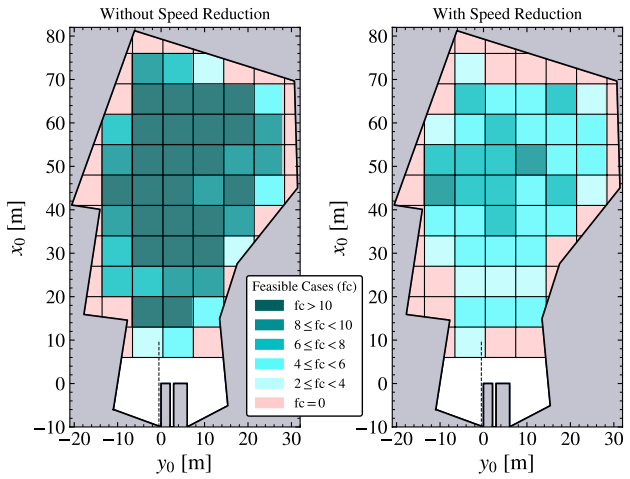

Fig. 18 Distribution cases with feasible solutions across the port geometry for simulations performed with and without speed reduction constraints

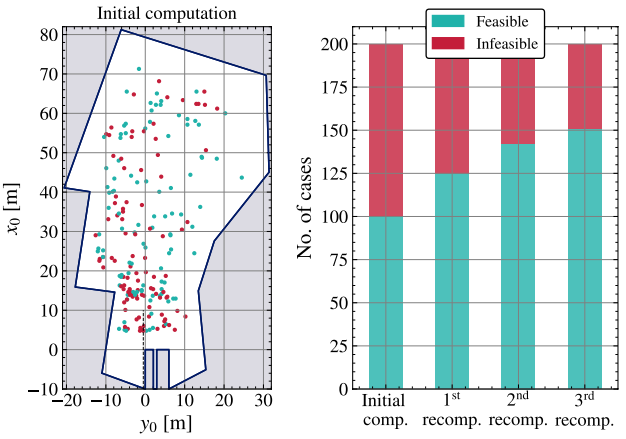

Fig. 20 Distribution of the stochastic initial conditions, where 50% of the cases were feasible in the initial computation. The histogram illustrates the changes in feasibility status after the recomputation attempts, with 50%, 62.5%, 71%, and 75% of the cases found feasible in the initial computation, first, second, and third recomputations, respectively

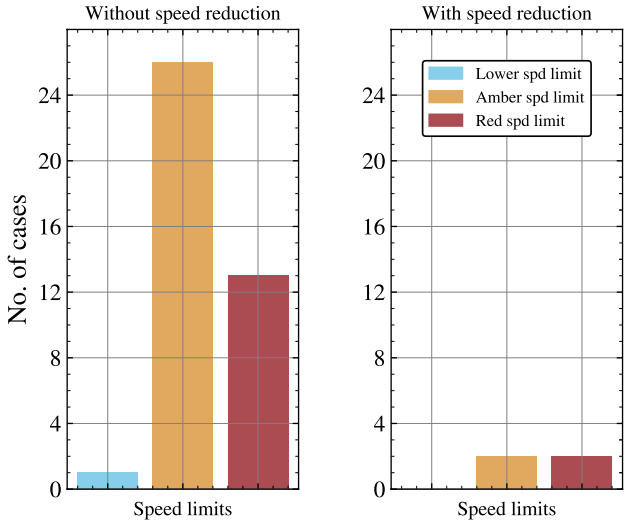

Fig. 19 Histograms illustrating the distribution of feasible cases that violate speed limits for simulations performed with and without speed reduction constraints

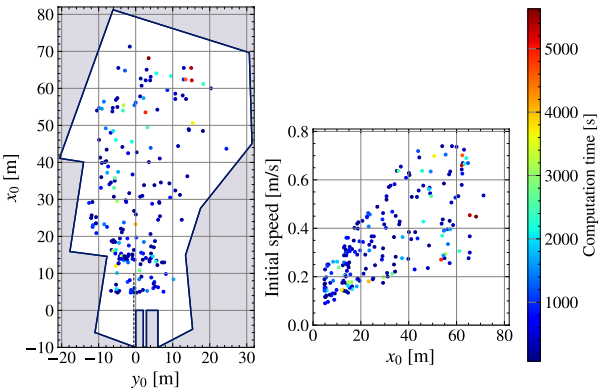

Fig. 21 Summary of computation time at the final computation attempt across all 200 cases, illustrating how computation time varies with distance from the berth and initial speed

Figure 21 shows how the computation speed varies for the stochastically generated cases regardless of their feasibility status. It is noteworthy that the initial computation time was less than 300 s for 71 cases. However, after the subsequent recomputation attempts, the total computation time per case increased, with the highest computation time being 5632 s. Moreover, the proposed planner can generate physically and dynamically feasible solutions in as little as 69 s for a case closest to the berth and 274 s for a case farthest from the berth.

4 Discussion and limitations

The proposed planner demonstrates a noteworthy departure from previous studies on the utilization of a simple linear guess to initialize the SQP algorithm. The simulation results in Figs. 11, 12, 13, 14, 15, 16, demonstrate the potential of using a less sophisticated initial guess for satisfactory performance of the trajectory planner. Moreover, the proposed planner demonstrates the ability to generate feasible solutions with a computation time of approximately 300 s or less for most cases, as detailed in Sects. 3.2 and 3.3. This computational efficiency presents a significant advantage in scenarios necessitating frequent

recomputation due to fluctuations in initial conditions or the infeasibility of previously generated solutions.

The inclusion of speed reduction and actuator limitations in NLP enhances the realism of the proposed trajectory planner. Although identical initial guesses were used for each case, significant differences were observed in the resulting optimal trajectories and deceleration patterns between simulations conducted with speed reduction constraints and those without. Further, from Figs. 11 12, 13, 14, 15, 16, a comparison between solutions obtained with and without speed reduction constraints indicates that, in the vicinity of the berth, simulations without speed reduction result in the ship approaching the berth within the '**Amber**' region, which poses a significant risk to ship handling. Moreover, as observed in Fig. 15, the absence of speed constraints can result in the ship decelerating to critically low speeds, rendering it incapable of effectively countering external disturbances. This condition poses a significant collision risk, particularly when the ship is in proximity to obstacles with limited time and space to accelerate and execute collision avoidance maneuvers. Therefore, while insufficient deceleration is not the sole factor leading to loss of control, incorporating speed reduction criteria in trajectory optimization is crucial and is guaranteed to enhance berthing safety. Moreover, accounting for actuator limitations during trajectory optimization introduces a buffer margin, enabling the system to counteract unknown disturbances while maintaining the ability to trace the generated trajectories.

In the grid-based feasibility study, the distribution of feasible cases was observed across the port geometry, with a higher concentration of feasible cases observed further from the port wall. This outcome is expected, as the collision avoidance constraints are more readily satisfied in regions with fewer spatial limitations. On the other hand, the number of feasible cases significantly decreased when the initial positions were closer to the port wall, where the collision risk was inherently higher. Additionally, when speed reduction constraints were incorporated, the number of feasible cases decreased, as the speed reduction criteria required substantial deceleration and initial speeds that satisfied the speed constraints. This added constraint made it more challenging to satisfy the optimization conditions. Further, in the feasibility study utilizing stochastic initial conditions, only 50% of the cases were initially feasible. However, significant improvements in feasibility were observed following three recomputations for the initially infeasible cases, ultimately achieving a 75% feasibility rate. The infeasibility rate can be partially attributed to practically unrealistic initial positions and headings. Nonetheless, the outcomes of the feasibility study highlight the planner's capability to generate practically viable solutions across a wide range of diverse initial conditions, demonstrating its adaptability and reliability in varying scenarios.

Despite these promising results, the proposed trajectory planner has certain limitations. The utilization of a simple linear guess to initialize the SQP may be insufficient in a complex port geometry or in the presence of wind gusts and dynamic obstacles commonly encountered in harbor settings, such as moving ships or floating debris. This situation may require the introduction of strategically determined waypoints, whereby the linear guess used to initialize the SQP is constructed from a sequence of linear interpolations of state variables between consecutive waypoints, as opposed to interpolating directly between the initial and terminal states, as demonstrated in the current study. It is anticipated that the proposed planner will remain capable of generating feasible solutions in this context. Evaluating the performance of the proposed planner in such complex scenarios, and considering wind gusts is part of future research.

Additionally, from the feasibility study, it was observed that changing only the control input guess during recomputation may not adequately improve the overall feasibility. This necessitates the exploration of alternative strategies, such as modifying the initial heading or speed relative to wind direction, given the well-established influence of prevailing wind speed and direction on the ship's trajectory [27], heading [48], and speed [49]. Furthermore, the initial control guess was derived through trial and error. Future research will focus on deriving the initial control guess from actual ship data, which is expected to substantially improve the algorithm's performance by providing more accurate and realistic initialization for the SQP.

Moreover, although the computation time required for most cases was less than 300 s, the introduction of recomputation significantly increased the computation time to as high as 5000 s in some cases. This increase in computational burden, while addressing infeasibility, may pose challenges in real-time applications. Future work will include further refinement of the proposed trajectory planner to enhance its robustness and adaptability in practical applications.

5 Conclusion

In summary, this study presented a robust trajectory planner tailored for the autonomous berthing process, with a primary focus on enhancing safety. In addition to ensuring compliance with regulatory requirements, the implemented speed reduction criterion was shown to improve berthing safety and facilitate a controlled approach to the berth. The incorporation of a rate of change and artificial limitations on the actuators accounted for their physical constraints, thereby reinforcing the planner's viability for practical applications. Moreover, the utilization of a ship domain to define collision avoidance constraints increased the safety clearance margin, significantly reducing the likelihood of collisions with port

structures. Finally, the feasibility study demonstrated that the proposed trajectory planner was not only theoretically sound but also practically applicable.

Acknowledgements This work was supported by a Grant-in-Aid for Scientific Research from the Japan Society for Promotion of Science (JSPS KAKENHI Grant Number 22H01701).

Funding Open Access funding provided by Osaka University.

Data availability The authors do not have permission to share data used in this study.

Declarations

Conflict of interest The authors declare that they have no Conflict of interest.

References

1. Inoue K, Hiroaki S, Kenji M (2002) Guidelines for speed reduction in berthing manoeuvre. J Japan Institute Navig pp 169–176
2. Chang YT, Park H (2019) The impact of vessel speed reduction on port accidents. Accident Anal Prevent 123:422–432. https://doi.org/10.1016/j.aap.2016.03.003
3. International Maritime Organization (IMO) (2003) COLREG: Convention on the International Regulations for Preventing Collisions at Sea, 1972. IMO Publication, International Maritime Organization, https://books.google.co.jp/books?id=_ZkZAQAAIAAJ
4. Hara K (1976) Deceleration pattern when entering port by operator's perception model. J Japan Institute Navig 55:53–61
5. Inoue K, Hanabusa M (1991) Assessment of safety margin of approach manoeuvre. J Japan Institute Navig 84:37–44. https://doi.org/10.9749/jin.84.37
6. European Maritime Safety Agency (EMSA) (2023) Annual overview of marine casualties and incidents 2023. https://emsa.europa.eu/publications/download/7639/5052/23.html
7. Fossen TI (2011) Handbook of marine craft hydrodynamics and motion control. John Willy & Sons Ltd
8. Öztürk Ülkü, Akdağ M, Ayabakan T (2022) A review of path planning algorithms in maritime autonomous surface ships: navigation safety perspective. Ocean Eng 251:111010. https://doi.org/10.1016/j.oceaneng.2022.111010
9. Zhang Hy, Lin Wm, Chen Ax (2018) Path planning for the mobile robot: a review. Symmetry 10(10). https://doi.org/10.3390/sym10100450, https://www.mdpi.com/2073-8994/10/10/450
10. Hart PE, Nilsson NJ, Raphael B (1968) A formal basis for the heuristic determination of minimum cost paths. IEEE Trans Syst Sci Cybernet 4(2):100–107
11. Hart PE, Nilsson NJ, Raphael B (1972) Correction to" a formal basis for the heuristic determination of minimum cost paths". ACM SIGART Bull 37:28–29
12. Liu C, Mao Q, Chu X, Xie S (2019) An improved a-star algorithm considering water current, traffic separation and berthing for vessel path planning. Appl Sci 9:1057. https://doi.org/10.3390/app9061057
13. Yuan S, Liu Z, Sun Y, Wang Z, Zheng L (2023) An event-triggered trajectory planning and tracking scheme for automatic berthing of unmanned surface vessel. Ocean Eng 273:113964. https://doi.org/10.1016/j.oceaneng.2023.113964
14. Maki A, Sakamoto N, Akimoto Y, Nishikawa H, Umeda N (2020) Application of optimal control theory based on the evolution strategy (cma-es) to automatic berthing. J Marine Sci Technol 25:221–233
15. Hansen N (2006) The cma evolution strategy: a comparing review. Advances in the estimation of distribution algorithms, Towards a new evolutionary computation, pp 75–102
16. Sakamoto N, Akimoto Y (2017) Modified box constraint handling for the covariance matrix adaptation evolution strategy. In: Proceedings of the Genetic and Evolutionary Computation Conference Companion, pp 183–184
17. Miyauchi Y, Sawada R, Akimoto Y, Umeda N, Maki A (2022) Optimization on planning of trajectory and control of autonomous berthing and unberthing for the realistic port geometry. Ocean Eng 245:110390. https://doi.org/10.1016/j.oceaneng.2021.110390
18. Suyama R, Miyauchi Y, Maki A (2022) Ship trajectory planning method for reproducing human operation at ports. Ocean Eng 266:112763. https://doi.org/10.1016/j.oceaneng.2022.112763
19. Koyama T, Yan J, Huan JK (1987) A systematic study on automatic berthing control (1st report). J Soc Naval Archit Japan 162:201–210
20. Yamato H, Koyama T, Nakagawa T (1993) Automatic berthing system using expert system. J Soc Naval Archit Japan 174:327–337
21. Shouji K, Ohtsu K, Mizoguchi S (1992) An automatic berthing study by optimal control techniques. IFAC Proc Vol 25(3):185–194
22. Wu A, Miele A (1980) Sequential conjugate gradient-restoration algorithm for optimal control problems with non-differential constraints and general boundary conditions, part i. Optim Control Appl Methods 1(1):69–88
23. Djouani K, Hamam Y (1995) Minimum time-energy trajectory planning for automatic ship berthing. IEEE J Ocean Eng 20(1):4–12. https://doi.org/10.1109/48.380251
24. Khatib O (1986) Real-time obstacle avoidance for manipulators and mobile robots. Int J Robot Res 5(1):90–98
25. Liao Y, Jia Z, Zhang W, Jia Q, Li Y (2019) Layered berthing method and experiment of unmanned surface vehicle based on multiple constraints analysis. Appl Ocean Res 86:47–60. https://doi.org/10.1016/j.apor.2019.02.003
26. Han S, Wang L, Wang Y (2022) A potential field-based trajectory planning and tracking approach for automatic berthing and colregs-compliant collision avoidance. Ocean Eng 266:112877. https://doi.org/10.1016/j.oceaneng.2022.112877
27. Mizuno N, Uchida Y, Okazaki T (2015) Quasi real-time optimal control scheme for automatic berthing. IFAC-PapersOnLine 48:305–312. https://doi.org/10.1016/J.IFACOL.2015.10.297
28. Zhang M, Yu SR, Chung KS, Chen ML, Yuan ZM (2023) Time-optimal path planning and tracking based on nonlinear model predictive control and its application on automatic berthing. Ocean Eng 286:115228. https://doi.org/10.1016/j.oceaneng.2023.115228
29. Martinsen AB, Bitar G, Lekkas AM, Gros S (2020) Optimization-based automatic docking and berthing of asvs using exteroceptive sensors: Theory and experiments. IEEE Access 8:204974–204986

30. Bitar G, Vestad VN, Lekkas AM, Breivik M (2019) Warm-started optimized trajectory planning for asvs. IFAC-PapersOnLine 52(21):308–314, https://doi.org/10.1016/j.ifacol.2019.12.325, 12th IFAC Conference on Control Applications in Marine Systems, Robotics, and Vehicles CAMS 2019
31. Rachman DM, Maki A, Miyauchi Y, Umeda N (2022) Warm-started semionline trajectory planner for ship's automatic docking (berthing). Ocean Eng 252:111127
32. Wang X, Deng Z, Peng H, Wang L, Wang Y, Tao L, Lu C, Peng Z (2023) Autonomous docking trajectory optimization for unmanned surface vehicle: a hierarchical method. Ocean Eng 279:114156. https://doi.org/10.1016/j.oceaneng.2023.114156
33. Vagale A, Bye RT, Oucheikh R, Osen OL, Fossen TI (2021) Path planning and collision avoidance for autonomous surface vehicles ii: a comparative study of algorithms. J Marine Sci Technol 26(4):1307–1323
34. Chang YT, Park H (2019) The impact of vessel speed reduction on port accidents. Accident Anal Prevent 123:422–432
35. Rachman DM, Aoki Y, Miyauchi Y, Umeda N, Maki A (2023) Experimental low-speed positioning system with vectwin rudder for automatic docking (berthing). J Marine Sci Technol 28(3):689–703
36. Yoshimura Y, Nakao I, Ishibashi A (2009) Unified mathematical model for ocean and harbour manoeuvring. International Conference on Marine Simulation and Ship Maneuverability, pp 116–124, http://hdl.handle.net/2115/42969
37. Yasukawa H, Yoshimura Y (2015) Introduction of mmg standard method for ship maneuvering predictions. J Marine Sci Technol (Japan) 20:37–52. https://doi.org/10.1007/s00773-014-0293-y
38. Kang D, Nagarajan V, Hasegawa K, Sano M (2008) Mathematical model of single-propeller twin-rudder ship. J Marine Sci Technol 13:207–222
39. Fujiwara T, Ueno M, Nimura T (1998) Estimation of wind forces and moments acting on ships. J Soc Naval Archit Japan 183:77–90
40. Maki A, Akimoto Y, Naoya U (2021) Application of optimal control theory based on the evolution strategy (cma-es) to automatic berthing (part: 2). J Marine Sci Technol 26:835–845
41. Betts JT (1998) Survey of numerical methods for trajectory optimization. J Guidance Control Dynam 21(2):193–207
42. Diehl M, Bock HG, Diedam H, Wieber PB (2006) Fast direct multiple shooting algorithms for optimal robot control. Fast motions in biomechanics and robotics: optimization and feedback control pp 65–93
43. Puchaud P, Bailly F, Begon M (2023) Direct multiple shooting and direct collocation perform similarly in biomechanical predictive simulations. Computer Methods Appl Mech Eng 414:116162. https://doi.org/10.1016/j.cma.2023.116162
44. García-Heras J, Soler M, Sáez FJ (2014) A comparison of optimal control methods for minimum fuel cruise at constant altitude and course with fixed arrival time. Procedia Eng 80:231–244
45. Kose K, Fukudo J, Sugano K, Akagi S, Harada M (1986) On a computer aided maneuvering system in harbours. J Soc Naval Archit Japan 160:103–110
46. Hormann K, Agathos A (2001) The point in polygon problem for arbitrary polygons. Comput Geom 20(3):131–144
47. National Research Council (1981) Problems and Opportunities in the Design of Entrances to Ports and Harbors: Proceedings of a Symposium
48. Wu G, Li D, Ding H, Shi D, Han B (2023) An overview of developments and challenges for unmanned surface vehicle autonomous berthing. Complex Intellig Syst. https://doi.org/10.1007/s40747-023-01196-z
49. Guard, Japan Coast (2010) New rules for maritime traffic safety. http://www.kaiho.mlit.go.jp/03kanku/h22houkaisei/indexhtm/